Strong carrier localization and diminished quantum-confined Stark effect in ultra-thin high-indium-content InGaN quantum wells with violet light emission

Suk-Min Ko, Ho-Sang Kwack, Chunghyun Park, Yang-Seok Yoo, Soon-Yong Kwon, Hee Jin Kim, Euijoon Yoon, Le Si Dang, and Yong-Hoon Cho

Citation: Applied Physics Letters **103**, 222104 (2013); doi: 10.1063/1.4833917
View online: http://dx.doi.org/10.1063/1.4833917
View Table of Contents: http://scitation.aip.org/content/aip/journal/apl/103/22?ver=pdfcov
Published by the AIP Publishing

Strong carrier localization and diminished quantum-confined Stark effect in ultra-thin high-indium-content InGaN quantum wells with violet light emission

Suk-Min Ko,[1] Ho-Sang Kwack,[1] Chunghyun Park,[1] Yang-Seok Yoo,[1] Soon-Yong Kwon,[2,4] Hee Jin Kim,[2] Euijoon Yoon,[2,a)] Le Si Dang,[3] and Yong-Hoon Cho[1,b)]
[1]*Department of Physics and KI for the NanoCentury, Korea Advanced Institute of Science and Technology, Daejeon 305-701, Korea*
[2]*Department of Materials Science and Engineering, Seoul National University, Seoul 151-744, Korea*
[3]*Nanophysics and Semiconductors, CEA-CNRS-UJF Group, Institut Néel, CNRS Grenoble, 25 rue des Martyrs, 38042 Grenoble Cedex 9, France*
[4]*School of Mechanical and Advanced Materials Engineering, Ulsan National Institute of Science and Technology, Ulsan 689-798, Korea*

(Received 18 September 2013; accepted 10 November 2013; published online 25 November 2013)

Here, we report on the optical and structural characteristics of violet-light-emitting, ultra-thin, high-Indium-content (UTHI) InGaN/GaN multiple quantum wells (MQWs), and of conventional low-In-content MQWs, which both emit at similar emission energies though having different well thicknesses and In compositions. The spatial inhomogeneity of In content, and the potential fluctuation in high-efficiency UTHI MQWs were compared to those in the conventional low-In-content MQWs. We conclude that the UTHI InGaN MQWs are a promising structure for achieving better quantum efficiency in the visible and near-ultraviolet spectral range, owing to their strong carrier localization and reduced quantum-confined Stark effect. © *2013 AIP Publishing LLC*.
[http://dx.doi.org/10.1063/1.4833917]

Recent advances in group III-nitride semiconductors and their heterostructures have made possible the commercial production of optoelectronic devices such as light emitting diodes, laser diodes, high electron mobility transistors, and solar cells.[1,2] Among these, the InGaN alloy structures are the most important materials for high efficiency light sources because of their direct band-gap and a wide spectral region (ultraviolet to infrared). The main reason for the high quantum efficiency of the InGaN alloy despite high threading dislocation density of over $10^8\,cm^{-2}$ caused by lattice misfit between GaN and sapphire substrate and severe built-in electric field of a few MV/cm due to the spontaneous and piezoelectric polarizations is generally known as the strong exciton localization trapped by lattice-parameter-scale In-N clusters in the random InGaN alloy.[3,4] Nevertheless, violet-emitting (390 nm) conventional low-In-content InGaN/GaN multi-quantum wells (MQWs) show the degradation in internal quantum efficiency compared to blue-emitting (450 nm) MQWs owing higher In-content due to the less localization of carrier and the smaller band offset. We expected that an improvement of internal quantum efficiency in the violet region can be achieved by replacing the conventional low-In-content InGaN/GaN MQWs with ultra-thin, high-In-content (UTHI) InGaN/GaN MQWs because of better localization of carriers and smaller quantum-confined Stark effect (QCSE). However, growth of UTHI MQWs is still very difficult due to the In-segregation problem and the interfacial roughness caused by the spatial inhomogeneity of strain. Recent growth of InN materials is also strongly progressive and indicative of potential device application.[5,6] Again, this is in spite of the difficulties of the growth of high quality InN film because of its thermal instability and the lattice mismatch between GaN and InN (~11%). Using these kinds of InN growth techniques, an improvement of interfacial abruptness and a reduction of well thickness in high-In-content InGaN/GaN heterostructures by the decomposition and mass transport process during growth interruption (GI) has been accomplished.[6] In this work, we investigated the optical and structural properties of the UTHI InGaN/GaN MQWs grown via employing the GI technique in comparison with conventional low-In-content InGaN/GaN MQWs. Stronger localization of carriers and smaller QCSE were observed in UTHI MQWs as a result of enlarged potential fluctuation and thinner QW thickness compared to those in conventional low-In-content MQWs. These strong carrier localization and reduced QCSE can turn the UTHI InGaN/GaN MQWs into an attractive candidate for high efficient violet emitter.

The UTHI InGaN/GaN MQWs were grown on a *c*-plane sapphire substrate by metal-organic chemical vapor deposition. The structure consists of a 2-μm-thick GaN buffer-layer grown at 1080 °C and eight-period In-rich InGaN (1 nm)/GaN (10 nm) MQWs (sample A) grown at 730 °C; using GI for a period of 10 s before GaN capping. During the growth of QW layer, only trimethylindium and ammonia were supplied as precursors to produce InN. However, solid-state intermixing of InN with underlying and capping GaN layers occurred during growth. Consequently high-In-content InGaN QW with compositional grading of indium along growth direction (*c*-axis) was formed, instead of InN QW. This was determined by medium ion energy scattering (MEIS) measurement.[7] For comparison, conventional low-In-content $In_yGa_{1-y}N$ (3 nm, $y \approx 0.1$, 790 °C, 100 s)/GaN

a)Electronic mail: eyoon@snu.ac.kr.
b)Electronic mail: yhc@kaist.ac.kr.

(10 nm, 850 °C, 120 s) MQWs with eight periods (sample B) was grown on a 2-μm-thick GaN buffer-layer to provide a reasonable comparison between high-In-content (sample A) and low-In-content (sample B) InGaN/GaN MQWs. Both these emit at similar emission energies, while having different well thicknesses and In compositional profiles.

Transmission electron microscopy (TEM) images of both samples were taken using FEI Tecnai G^2 F30 S-Twin. 5 K (300 K) cathodoluminescence (CL) measurements were carried out using an FEI Quanta 200 (FEI Philips XL-30 SFEG) scanning electron microscopy with a liquid-He-cooled sample stage, and a liquid-nitrogen-cooled charge-coupled device (a Gatan mono CL4 system). Photoluminescence (PL) spectra were carried out using the 325 nm line of a continuous-wave He-Cd laser. Selectively excited PL and PL excitation (PLE) spectra were measured using quasimonochromatic light from a xenon lamp, dispersed by a monochromator.

Figures 1(a) and 1(b) show the TEM micrographs of the QWs of samples A and B. High-resolution (HR) TEM images were taken with the low electron-beam current ($<$100 A/cm^2) and within a relatively shorter time ($<$1 min) to avoid the damage on the surface of the specimen, which causes the strain-induced lattice distortion due to the high electron-beam current and the long irradiation time. As shown in Figs. 1(a) and 1(b), the thickness of the QWs of both samples are easily obtainable because of the obvious intensity contrast between the GaN and InGaN layers; however, the In concentration inside the QWs of both samples is not distinguishable due to the similar intensity contrast across the InGaN layer. The average thicknesses of the QWs of samples A and B were 1.045 nm and 3.098 nm, respectively. To evaluate the precise concentration and spatial distribution of indium inside the ultra-thin QW of sample A, the (0002) lattice fringe images were taken along the off-axis orientations of about 5° away from [1$\bar{1}$00]-zone axis of the sample A. Figure 1(c) shows the lattice-parameter map of sample A taken from the white-boxed regions (i1)−(i3) of Fig. 1(a).[8,9] The lattice parameter D was defined as $D = c_{0002}^{Measured} \div c_{0002}^{GaN}$, where $c_{0002}^{Measured}$ is the measured distance between the lattice fringes and c_{0002}^{GaN} is the half of the lattice constant c(2.593 Å) of the strain-free bulk GaN, respectively.[10] The In content is calculated with consideration of the linear dependency of the lattice parameter between GaN and InN (Vergard's law) and the tetragonal distortion due to the biaxial misfit strain.[9] The lattice parameter map in Fig. 1(c) shows the irregular distribution of indium along the lateral direction of UTHI QW in sample A, and the existence of the tiny In-rich In-N clusters. Most of the indium content of the QW ranges from 24% to 47%. Figures 1(d) and 1(e) are the averaged D values as a function of the scan positions across the white-boxed areas (i1)−(i3) of Fig. 1(a) and (j1)−(j3) of Fig. 1(b), respectively. As shown in Fig. 1(d), the UTHI InGaN wells have about three mono-layers (ML) 0.801 nm thick, which consist of 1 ML high-In-content InGaN well, with In content of 24%–47% in the middle of QW; and 1 ML InGaN well with In content of 17% and 8%, above and below the high-In-content layer at the center, respectively. There are two possible explanations for this compositional grading inside the InGaN well of sample A: the solid-state intermixing between InN and GaN capping/underlying layers and the compositional pulling effects.[7] The D value at the top of the GaN underlying barrier is smaller than the strain-fee GaN case (i.e., $D = 1$) because of the tetragonal distortion of GaN due to the

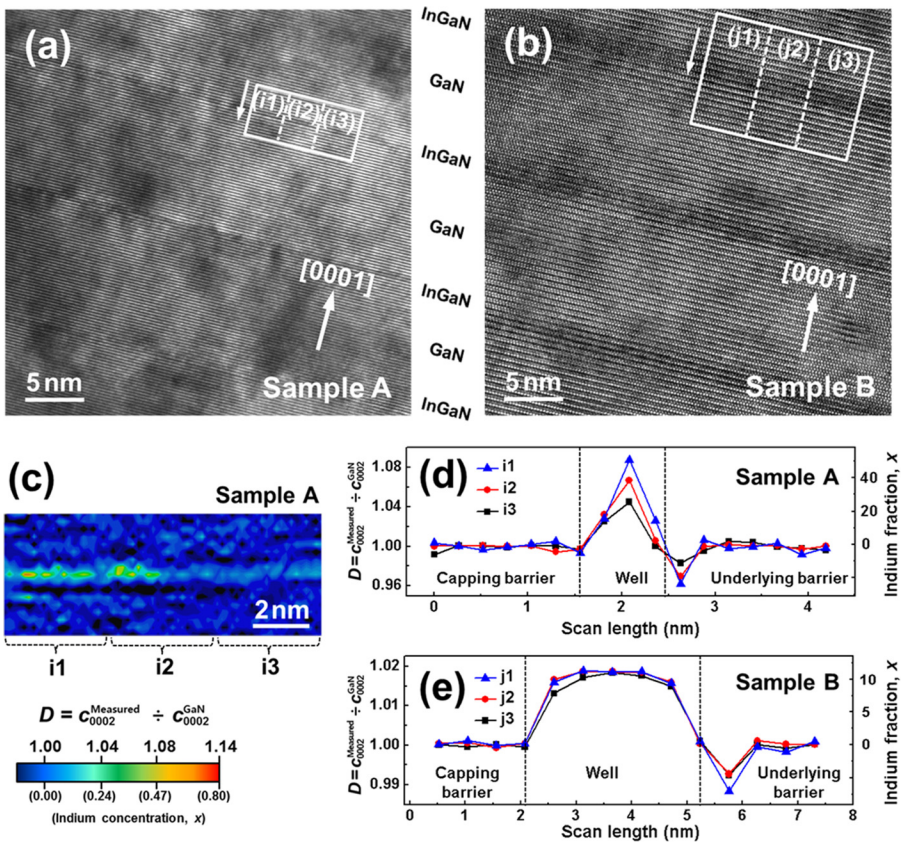

FIG. 1. HRTEM micrographs of the QWs of (a) sample A and (b) sample B. (c) The lattice parameter map of sample A taken from the white-boxed region. (c) and (d) The averaged lattice parameter across the white-boxed areas (i1−i3) of sample A and (j1−j3) of sample B, respectively.

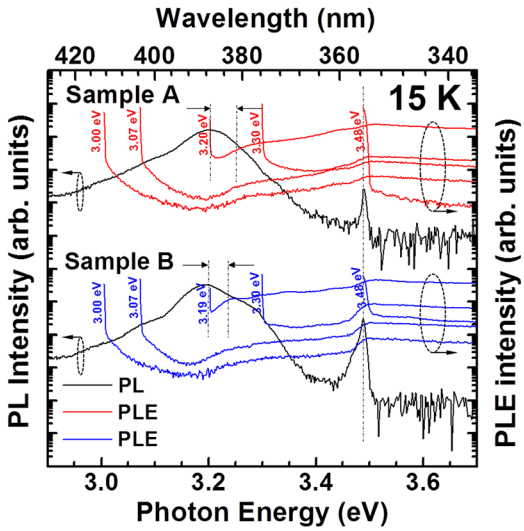

FIG. 2. PL and PLE spectra of samples A and B. The gaps between the two arrows confronting each other indicate the magnitude of Stokes shifts for samples A and B. The detection energies were included and indicated on each curve.

compressive misfit strain along the *c*-axis (i.e., tensile strain along the lateral direction). Contrary to UTHI InGaN QWs, low-In-content InGaN QWs have almost constant D (~10%) inside the QW without large compositional gradation in the upper and lower interface as shown in Fig. 1(e). Therefore, it is expected to have rougher interface between the InGaN well and the GaN barrier in sample A than that in sample B due to the large lateral In fluctuation and the huge compositional gradation inside the UTHI InGaN QW.

Figure 2 shows PL and PLE spectra of samples A and B measured at 15 K. In spite of much higher In content, the PL emission peak of sample A shifted to higher energy due to the stronger quantum confinement effect caused by extremely thin QW than that of sample B. Thus, the QW emission peaks of both samples are located at similar energies of ~3.2 eV. The PLE experiments were carried out at various detection energies including main QW emission energies of 3.202 eV for sample A and 3.194 eV for sample B. The values of the Stokes shift of samples A and B were estimated to be 46 meV and 25 meV via fitting PLE spectra, respectively. The magnitude of the Stokes shift in sample A is larger than that in sample B by 1.84 times because of the larger spatial potential fluctuation and higher In composition. Generally, it is known that the magnitude of Stokes shift is almost linearly proportional to In composition x and well thickness of $In_xGa_{1-x}N$ wells due to potential fluctuations and QCSE.[11] Thus, although the difference of x of $In_xGa_{1-x}N$ wells between samples A and B is almost sixfold, that of the Stokes shifts between two samples are less than twofold due to the ultra-thin QW thickness.

Figure 3 shows SEM images and monochromatic CL mapping images of QW emission for samples A and B. Although both samples show the brightest CL mapping images near the wavelength of 390 nm, the distribution of emission spots exhibit a marked difference in their spatial potential inhomogeneities between samples A and B. In the case of sample A, a great number of In-rich In-N clusters show the sub-micrometer-sized dot-like emissions at longer wavelength as shown in Fig. 3(d). The actual size of the In-N cluster might be much smaller than the observed sub-micrometer size of the dot-like emission spots since the lateral resolution of CL images is mainly limited by the electron-specimen interaction volume of several hundred nanometers due to the scattered and diffused electron inside the specimen. These high-density In-rich In-N clusters could be formed to relax strain energy inside the UTHI InGaN wells due to the large lattice mismatch between high-In-content InGaN and GaN. On the other hand, low-In-content InGaN wells on GaN barriers have lower strain energy compared to the case of UTHI InGaN wells. In the case of sample B, therefore, two-dimensional thin film growth along the terrace edge of GaN layer would be dominant, showing a line-shaped emission pattern, together with fewer In-rich In-N clusters with the sub-micrometer-sized dot-like emissions (marked by arrows) as shown in Fig. 3(h). A drastic and reverse contrast change in the distribution of emission spots was found for sample A in the CL images of Fig. 3(b) taken at 380 nm and Fig. 3(d) taken at 400 nm, whereas the emission distribution of sample B did not show any significant change as indicated by similar contrast correlations in the CL images of Figs. 3(f)–3(h). These results strongly reflect that carrier localization caused by strain inhomogeneity and In-N cluster formation is stronger in sample A than sample B, while sample B represents relatively uniform potential distribution along the lateral directions.

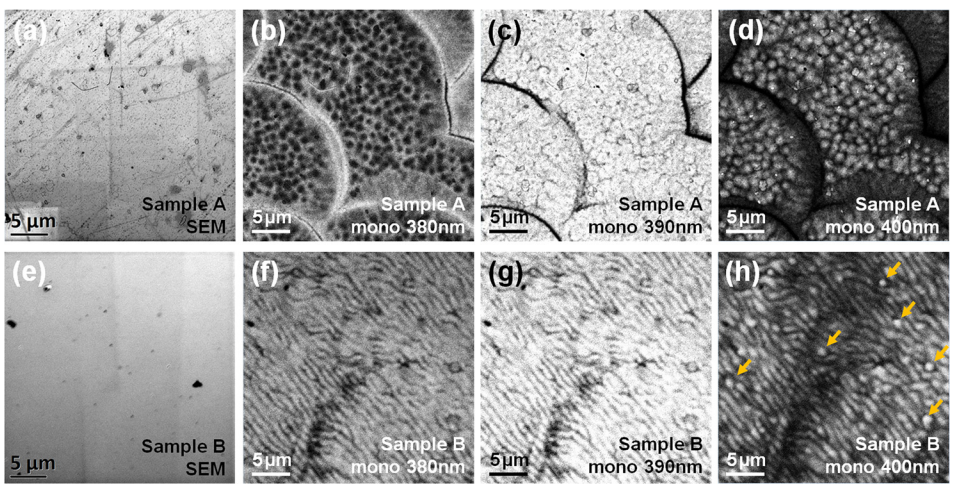

FIG. 3. SEM images and monochromatic CL images of samples A and B taken at the various wavelengths: (b), (f) 380 nm, (c), (g) 390 nm, and (d), (h) 400 nm. The CL intensity scale increases from black to white, so brighter area indicates stronger CL intensity in all the images.

Figure 4(a) indicates the CL spectra of sample A with different electron-beam accelerating voltages from 2 to 30 kV at an electron-beam current of 0.3 nA. As the accelerating voltage increased up to 30 kV, the emission energies and spectral shapes of MQW emission (~3.203 eV) are almost the same, except for the appearance of the near-band-edge and the donor-accepter-pair emission peaks from GaN. Figure 4(b) shows the 5 K CL spectra for sample A with varying electron-beam currents from 0.02 to 1.2 nA at an accelerating voltage of 20 kV. Generally, as total injected carrier density increases, the main MQW emission peak energy shifts to higher energy for conventional low-In-content InGaN/GaN MQWs due to the carrier screening and band filling effects.[12,13] However, an apparent peak shift in the CL spectra for sample A with increasing electron-beam current was not observed. To further investigate this behavior, the PL emission peak energy for sample A was also investigated with varying excitation power densities over three orders of magnitude at 15 K, as indicated in Fig. 4(c). This pump power density range was supposed to be sufficient to generate enough carriers to screen the internal electric field in the InGaN/GaN MQWs layers grown on sapphire substrate. However, the PL emission energies and the spectral shapes of sample A were almost the same with increasing excitation power. It is probably due to the diminished QCSE by ultra-thin QW thickness, the shrinkage of polarization-induced interface charge by the presence of the large In fluctuation, and high residual carrier density over 10^{18} cm^{-3} in UTHI InGaN QW, as most of the reported residual carrier densities in InN are in the order of 10^{18} to 10^{21} cm^{-3} (Ref. 14). In general, the band-filling effect due to In phase separation can cause the blue-shift behavior of the PL peak energies with increasing excitation intensity besides the carrier screening effect.[15] It is reasonable to infer from the above experimental results that the blue-shift of emission peak due to the band-filling effect may be partly compensated by the red-shift behavior associated with many body effect due to the high carrier density inside the InGaN well or by other carrier loss processes in sample A. On the contrary, sample B shows the common blue-shift behavior of PL emission peak energies by the gradual carrier screening by the photo-generated free carriers with increasing the laser power as shown in Fig. 4(d). It is due to the lower residual carrier density ($<10^{18}$ cm^{-3}) inside low-In-content InGaN well which could not cancel out the huge polarization field caused by larger QCSE without an assistance of the photo-generated free carriers.

Figure 5 show the evolution of InGaN-related QW PL spectra together with PL peak energy and full width at half maximum (FWHM) of the PL spectra for samples A and B over a temperature range of 15 to 300 K. The temperature dependence of PL peak energy for both samples A and B shows the "*S*-shaped" peak energy shift with increasing temperature. As shown in Figs. 5(c) and 5(d), the blue-shift behavior of the PL peak energy in sample A takes place at higher temperature than that of sample B. Generally, the crossover of the initial red-shift and blue-shift of PL peak energy arising with increasing temperature occurs at higher temperature for the samples with larger potential fluctuation or localization. When the depth of potential fluctuation is larger, the effective temperature at which carriers are thermally excited out of the potential minima is raised. These

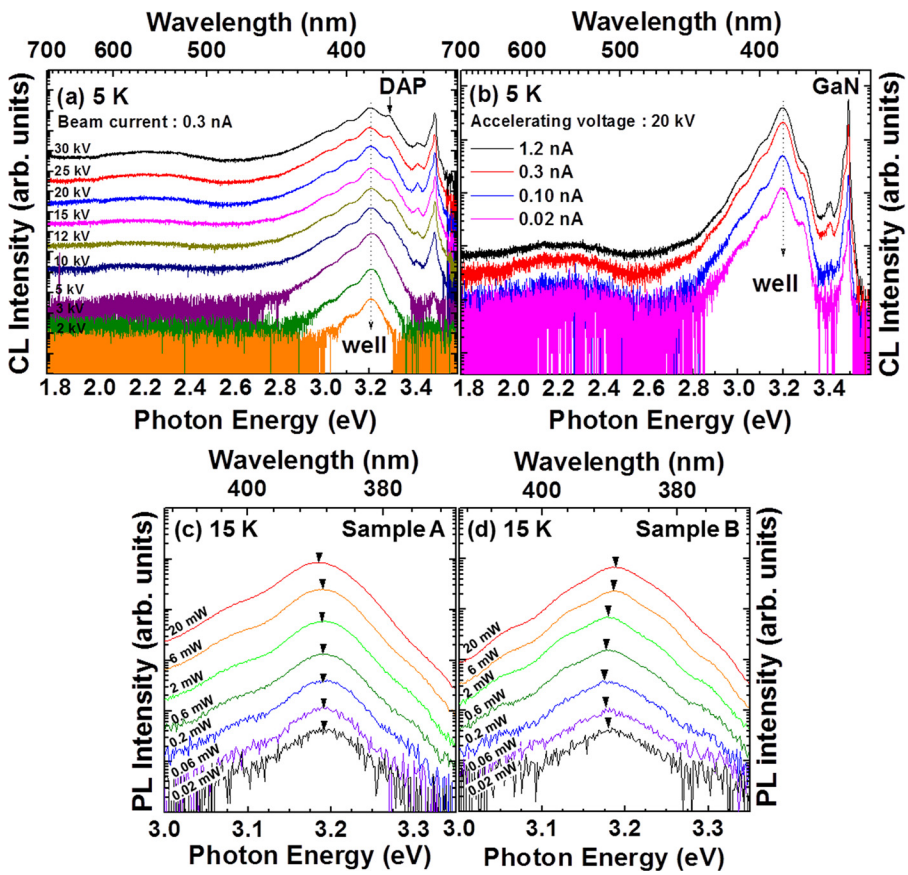

FIG. 4. (a) CL spectra of sample A with varying accelerating voltages from 2 to 30 kV. All the spectra in Fig. 4(a) are shifted in the vertical direction for clarity. (b) CL spectra of sample A with different injection currents from 0.02 to 1.2 nA. (c) and (d) PL spectra of samples A and B with varying excitation powers from 0.02 to 20 mW. Peak positions are indicated with inverted triangles.

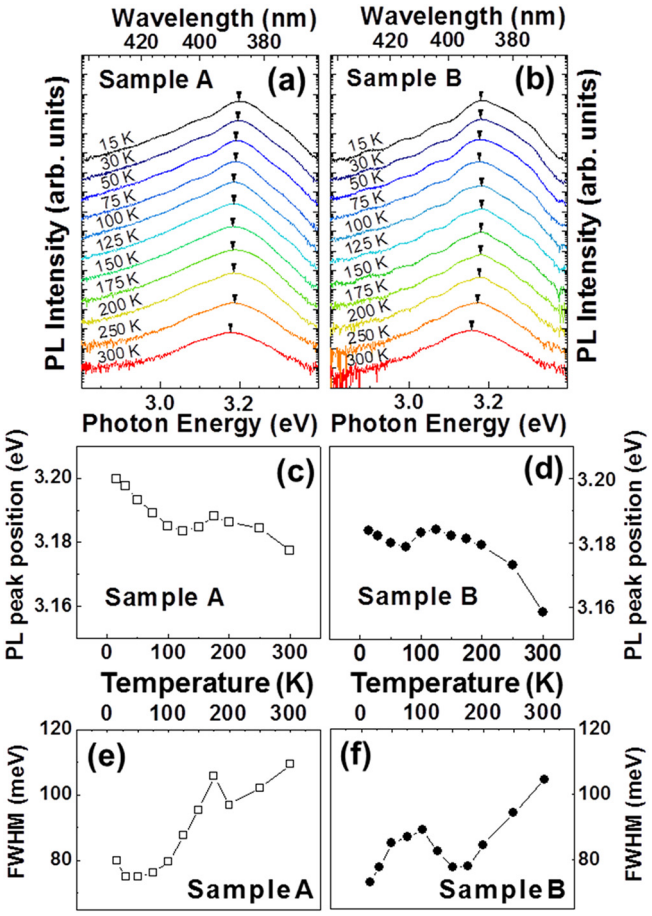

FIG. 5. PL spectra for (a) sample A and (b) sample B in the temperature range from 15 to 300 K. All the spectra are shifted in the vertical direction for clarity. The temperature dependence of the PL peak energy and the FWHM of the PL spectra of the InGaN-related emission is shown in (c) and (e) for sample A (open squares) and (d) and (f) for sample B (closed circles), respectively.

results agree well with the Stokes shifts obtained from the fitting of the PLE spectra (Fig. 2) and with the wavelength-resolved CL images (Fig. 3). The PL FWHM values of both samples show an inverted *S*-shape shift with temperature as shown in Figs. 5(e) and 5(f): the PL line-width is significantly broadened as temperature increases at low temperature region, becomes slightly narrow at the crossover temperature between initial red-shift and blue-shift of the PL peak position, and then is broadened again at sufficiently high temperature region showing final PL peak red-shift. The thermal activation energies of the InGaN-related luminescence associated with the degree of potential fluctuation are extracted from Arrhenius plots of both samples as 41.5 meV and 33.4 meV, respectively. Here, the higher thermal activation energy can be associated with larger effective potential fluctuation responsible for carrier localizations. Therefore, the larger potential fluctuation shown in sample A could provide an advantage in enhancing radiative recombination because of better localization of carriers inside the QW. In order to strengthen the advantages of UTHI InGaN/GaN MQWs itself such as small QCSE and superb localization of carriers, the density of defects existing in vicinity of In-N cluster should be reduced further by improving the GI techniques, resulting in much stronger carrier localization, less non-radiative carrier loss and hence better quantum efficiency.

In summary, the optical properties of violet-light-emitting UTHI InGaN/GaN MQWs (sample A) grown by employing the GI technique in comparison with conventional low-In-content InGaN/GaN MQWs (sample B) were investigated. No CL and PL blueshift was observed for sample A with increasing carrier density, reflecting a reduction of QCSE due to ultra-thin QW thickness. Sample A showed a stronger localization of carrier with a larger Stokes shift and high activation energy compared to those of sample B due to the larger potential fluctuation of the QWs. With a proper growth optimization the UTHI InGaN/GaN MQWs by employing GI technique may open up new approach to fabricate the high efficient near-ultraviolet solid-state light source with significant advantages mentioned above.

[1]J. K. Son, S. N. Lee, H. S. Paek, T. Sakong, H. K. Kim, Y. Park, H. Y. Ryu, O. H. Nam, J. S. Hwang, and Y. H. Cho, J. Appl. Phys. **103**, 103101 (2008).
[2]J. Simon, Z. Zhang, K. Goodman, H. Xing, T. Kosel, P. Fay, and D. Jena, Phys. Rev. Lett. **103**, 026801 (2009).
[3]S. F. Chichibu, A. Uedono, T. Onuma, B. A. Haskell, A. Chakraborty, T. Koyama, P. T. Fini, S. Keller, S. P. Denbaars, J. S. Speck, U. K. Mishra, S. Nakamura, S. Yamaguchi, S. Kamiyama, H. Amano, I. Akasaki, J. Han, and T. Sota, Nature Mater. **5**, 810 (2006).
[4]S. Zhang, J. Shi, S. Zhu, F. Wang, M. Yang, and Z. Bao, Phys. Lett. A **374**, 4767 (2010).
[5]A. Yoshikawa, S. B. Che, W. Yamaguchi, H. Saito, X. Q. Wang, Y. Ishitani, and E. S. Hwang, Appl. Phys. Lett. **90**, 073101 (2007).
[6]S.-Y. Kwon, H. J. Kim, H. Na, Y.-W. Kim, H.-C. Seo, H. J. Kim, Y. Shin, E. Yoon, and Y.-S. Park, J. Appl. Phys. **99**, 044906 (2006).
[7]S.-Y. Kwon, M.-H. Cho, P. Moon, H. J. Kim, H. Na, H.–C. Seo, H. J. Kim, Y. Shin, D. W. Moon, Y. Sun, Y.–H. Cho, and E. Yoon, Phys. Status Solidi A **201**, 2818 (2004).
[8]T. S. Smeeton, M. J. Kappers, J. S. Barnard, M. E. Vickers, and C. J. Humphreys, Appl. Phys. Lett. **83**, 5419 (2003).
[9]D. Gerthsen, E. Hahn, B. Neubauer, A. Rosenauer, O. Schön, M. Heuken, and A. Rizzi, Phys. Status. Solidi. A **177**, 145 (2000).
[10]S. Porowski, J. Cryst. Growth **189–190**, 153 (1998).
[11]S. Chichibu, T. Sota, K. Wada, and S. Nakamura, J. Vac. Sci. Technol. B **16**, 2204 (1998).
[12]B. Arnaudov, D. S. Domanevskii, S. Evtimova, C. Ivanov, and R. Kakanakov, Microelectron. J. **40**, 346 (2009).
[13]L. Wang, C. Lu, J. Lu, L. Liu, N. Liu, Y. Chen, Y. Zhang, E. Gu, and X. Hu, Opt. Express **19**, 14182 (2011).
[14]K. S. A. Butcher and T. L. Tansley, Superlattices Microstruct. **38**, 1 (2005).
[15]T. Mukai, M. Yamada, and S. Nakamura, Jpn. J. Appl. Phys., Part 1 **38**, 3976 (1999).